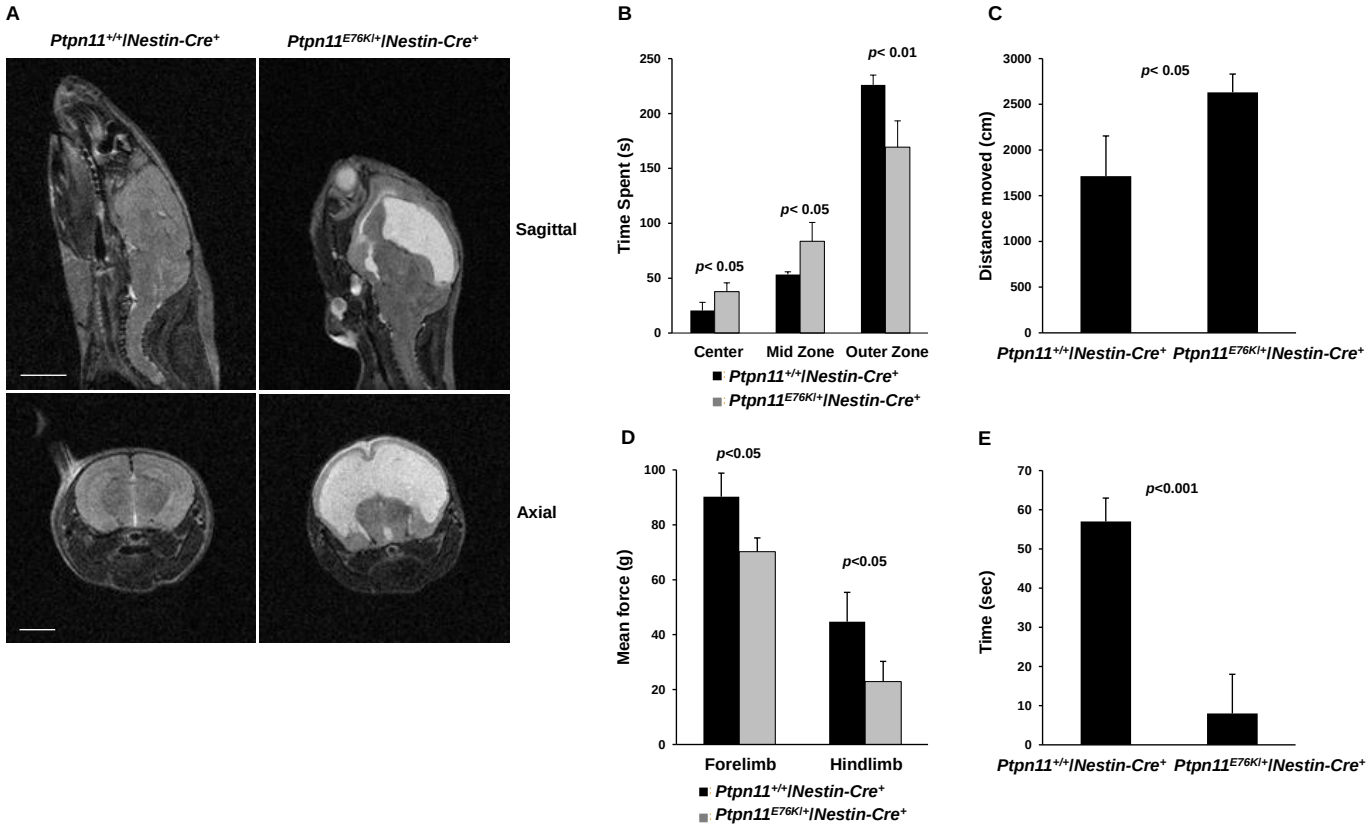

Fig. S1. The *Ptpn11*^{E76K} mutation induces brain developmental defects with aberrant behaviors. (**A**) T2-weighted sagittal and axial magnetic resonance imaging scans were performed on *Ptpn11*$^{E76K/+}$*/Nestin-Cre*$^{+}$ and *Ptpn11*$^{+/+}$ */Nestin-Cre*$^{+}$ mice (*n*=3 mice per genotype) at one month of age. (**B**-**E**) Behavioral profiles of male *Ptpn11*$^{E76K/+}$*/Nestin-Cre*$^{+}$ and *Ptpn11*$^{+/+}$*/Nestin-Cre*$^{+}$ littermates at 5-6 months of age (*n*=5 mice per genotype) were determined. The duration times mice spent in the center, mid zone, or outer zone (**B**), and the total distance mice moved (**C**) in open field tests were recorded. Mean forces of forelimbs and hindlimbs were measured in grip strength tests (**D**). The duration times mice hung on the wire before falling off were recorded in wire hang tests (**E**). Female *Ptpn11*$^{E76K/+}$*/Nestin-Cre*$^{+}$ and *Ptpn11*$^{+/+}$*/Nestin-Cre*$^{+}$ littermates at 5-6 months of age (*n*=4 mice per genotype) were also assessed. Analyses in all panels were performed in 3-4 independent experiments. Data are presented as mean±S.D. of biological replicates. Representative images are shown. Scale bars, 2 mm.

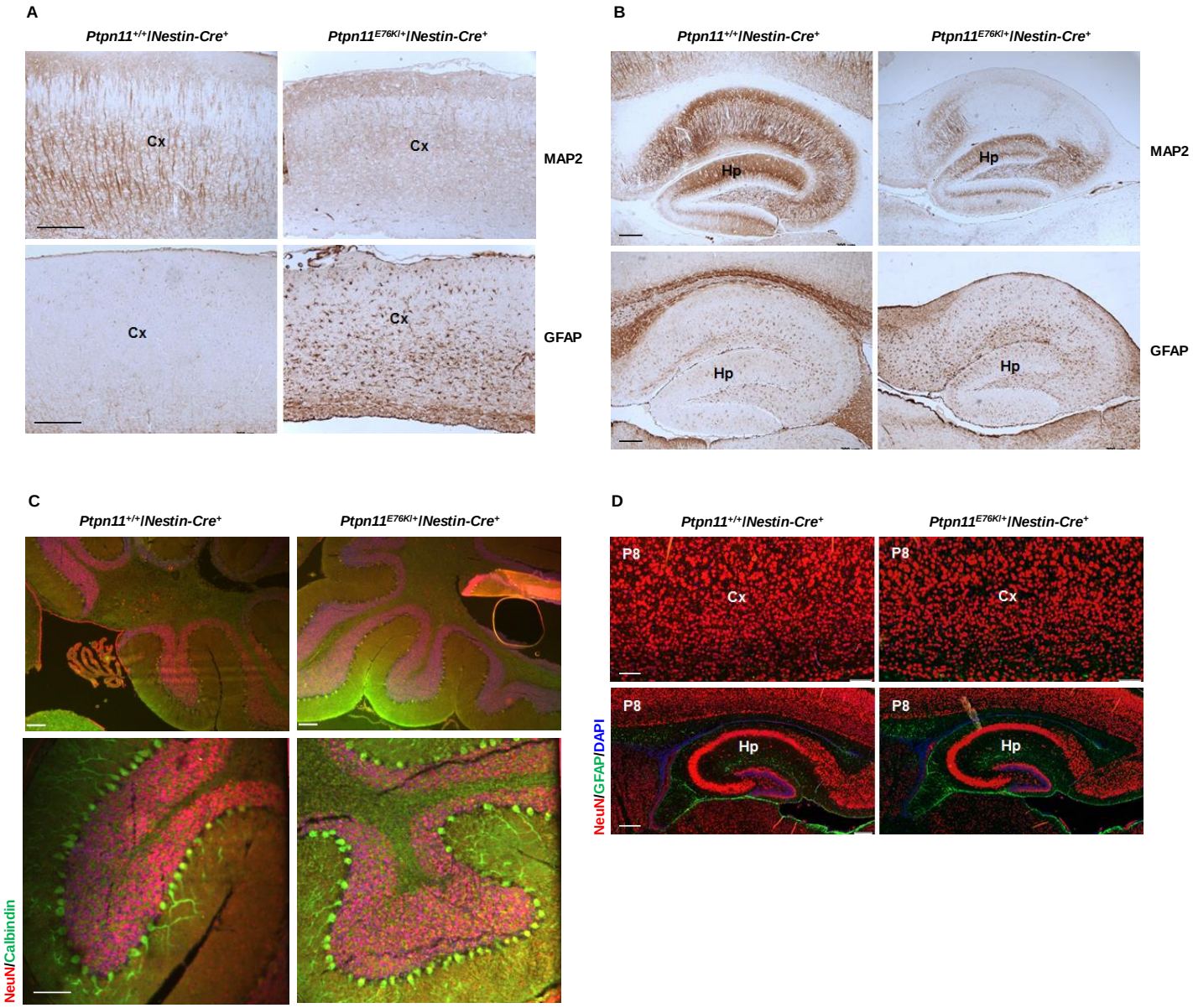

Fig. S2. Neurons are reduced, and astrocytes are increased in the cerebral cortex and hippocampus of adult *Ptpn11*$^{E76K/+}$*/Nestin-Cre*$^{+}$ mice. (**A** and **B**) Brain sections prepared from *Ptpn11*$^{E76K/+}$*/Nestin-Cre*$^{+}$ and *Ptpn11*$^{+/+}$*/Nestin-Cre*$^{+}$ mice (*n*=4 mice per genotype) at one month of age were processed for immunohistochemical staining to detect neurons (MAP2^{+}) and astrocytes (GFAP^{+}) in the cortex (**A**) and hippocampus (**B**). (**C**) Cerebellum sections prepared from *Ptpn11*$^{E76K/+}$*/Nestin-Cre*$^{+}$ and *Ptpn11*$^{+/+}$*/Nestin-Cre*$^{+}$ mice (*n*=4 mice per genotype) at one month of age were processed for immunofluorescence staining of Calbindin (Purkinje cells) and NeuN (granule neurons). (**D**) Brain sections prepared from P8 *Ptpn11*$^{E76K/+}$*/Nestin-Cre*$^{+}$ and *Ptpn11*$^{+/+}$*/Nestin-Cre*$^{+}$ mice (*n*=3 mice per genotype) were processed for immunofluorescence staining of NeuN (neurons) and GFAP (astrocytes). Cx, cortex; Hp, hippocampus. Analyses in all panels were performed in 3 independent experiments. Representative images are shown. Scale bars, 200μm (A, B, and D) and 100 μm (C).

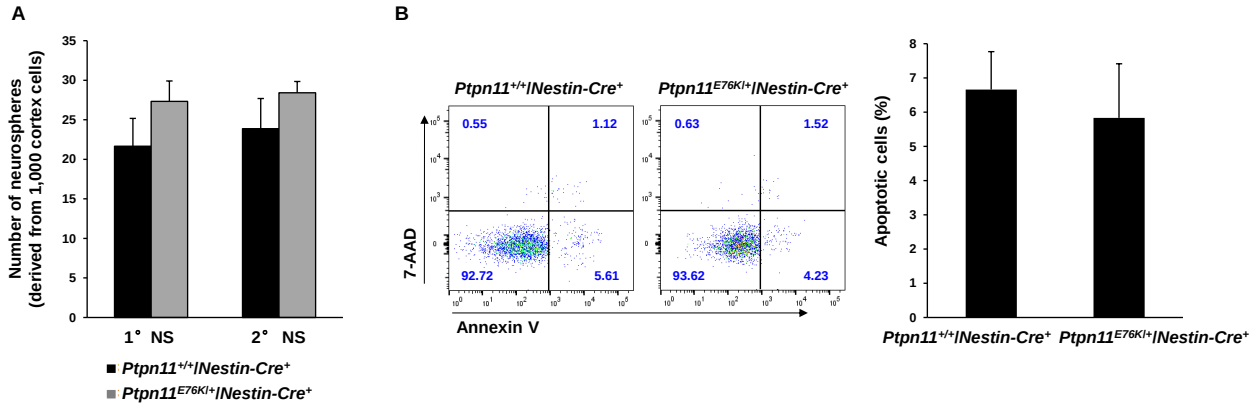

Fig. S3. Total number and survival of NSPCs in the developing brain of *Ptpn11*$^{E76K/+}$*/Nestin-Cre*$^{+}$ mice are not significantly changed. (**A**) Cerebral cortices dissected from E14.5 *Ptpn11*$^{E76K/+}$*/Nestin-Cre*$^{+}$ and *Ptpn11*$^{+/+}$*/Nestin-Cre*$^{+}$ embryos (n=4 mice per genotype) were assessed by neurosphere assays. Total number of primary neurospheres (1^0 NS) (big and small) was determined after 7 days of culture. Single cells dissociated from primary neurospheres were subjected to neurosphere assays again, and secondary neurospheres (2^0 NS) were quantified as above. (**B**) Primary neurospheres were harvested, dissociated into single cells, and examined for apoptotic cells by FACS analyses. Assays in all panels were conducted in 4 independent experiments. Data are presented as mean±S.D. of biological replicates.

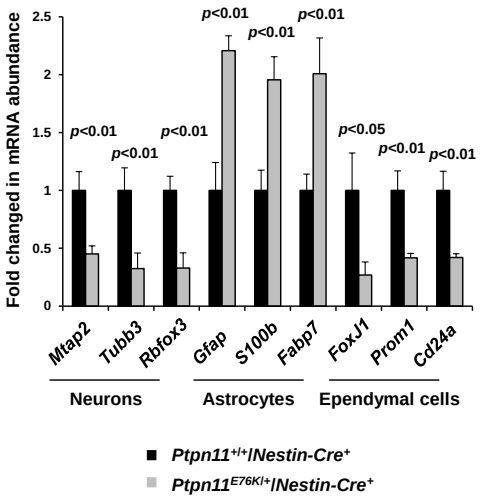

Fig. S4. Neuron and ependymal cell differentiation is decreased, whereas astrocyte differentiation is increased in *Ptpn11*$^{E76K/+}$*/Nestin-Cre*$^{+}$ NSPCs. Lateral ventricular walls were dissected from *Ptpn11*$^{E76K/+}$*/Nestin-Cre*$^{+}$ and *Ptpn11*$^{+/+}$*/Nestin-Cre*$^{+}$ newborn pups (*n*=3 mice per genotype), dissociated into single cells, and then processed for ependymal cell differentiation assays. The differentiated cells were harvested and subjected to real-time quantitative PCR analyses for mRNA abundance of the indicated cell lineage markers. Analyses were performed in 3 independent experiments. Data are presented as mean±S.D. of biological replicates.

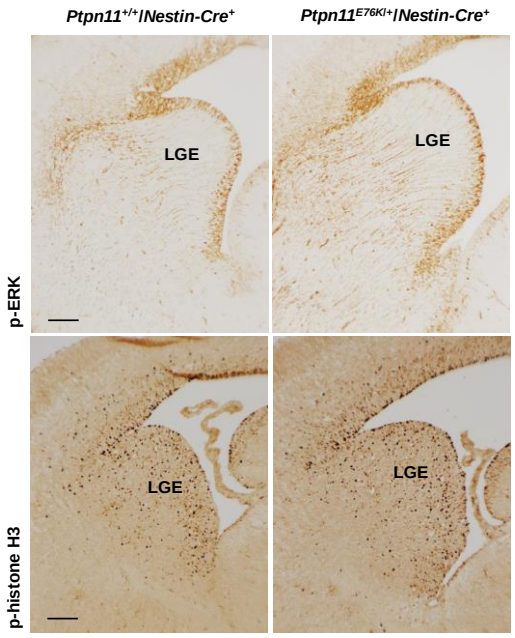

Fig. S5. ERK activity in the developing brain of *Ptpn11*$^{E76K/+}$*/Nestin-Cre*$^{+}$ mice is enhanced, but cell proliferation does not change. Brain sections prepared from E14.5 *Ptpn11*$^{E76K/+}$*/Nestin-Cre*$^{+}$ and *Ptpn11*$^{+/+}$*/Nestin-Cre*$^{+}$ embryos (*n*=3 mice per genotype) were processed for immunohistochemical staining of phosphorylated ERK (p-ERK) and phosphorylated hisone H3 (p-histone H3) in the lateral ganglionic eminence (LGE). Analyses were performed in 3 independent experiments. Representative images are shown. Scale bars, 100 μm.

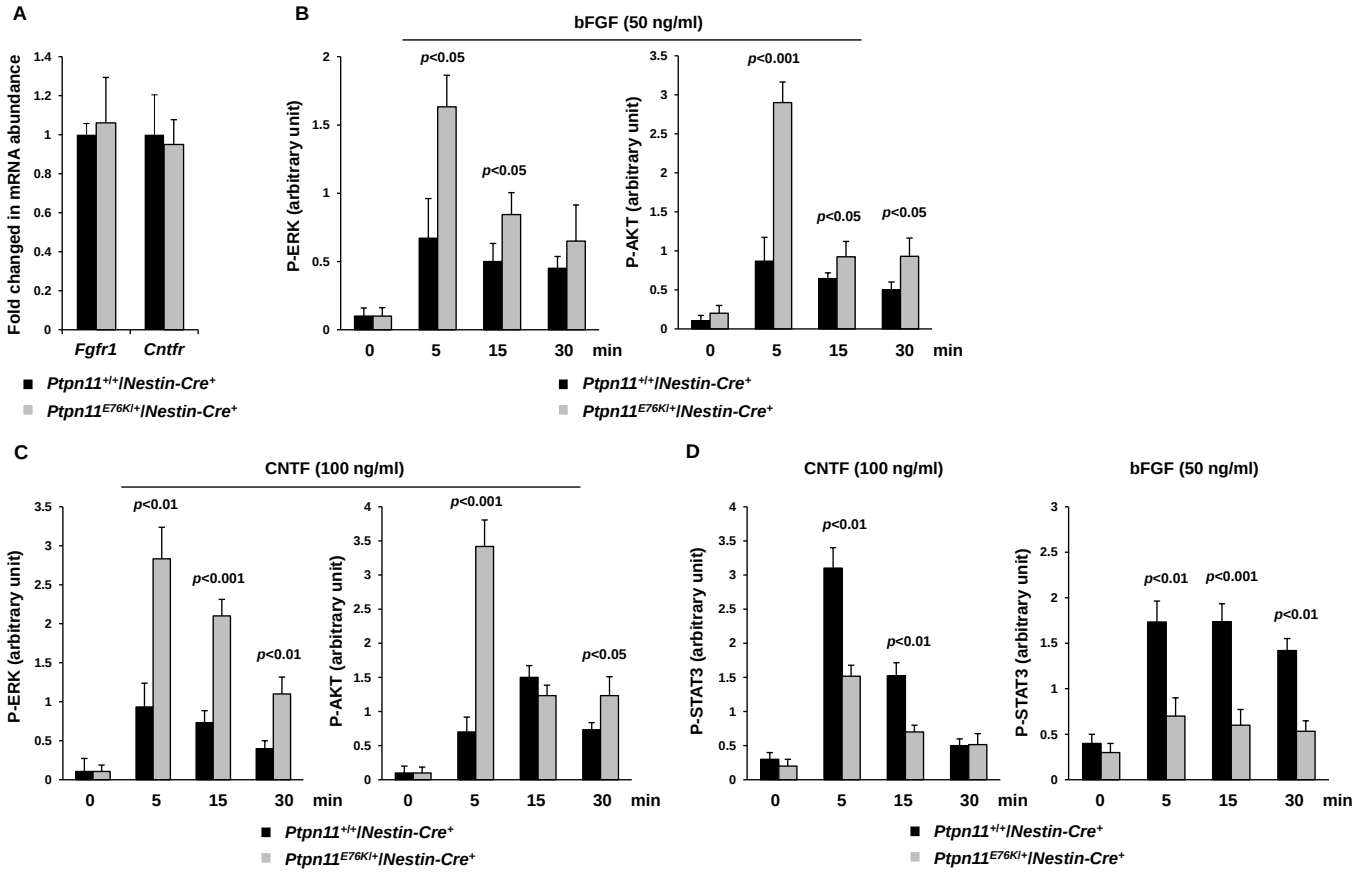

Fig. S6. Similar abundance of bFGF and CNTF receptors in *Ptpn11$^{E76K/+}$/Nestin-Cre^{+}* and *Ptpn11$^{+/+}$/Nestin-Cre^{+}* NSPCs. (**A**) Neurospheres were generated from E14.5 *Ptpn11$^{E76K/+}$/Nestin-Cre^{+}* and *Ptpn11$^{+/+}$/Nestin-Cre^{+}* embryos (*n*=3 mice per genotype). They were dissociated into single cells and cultured in the presence of bFGF (20 ng/ml) for 5 days. Cells were harvested and subjected to real-time quantitative PCR analyses for mRNA abundance of bFGFR and CNTFR. (**B**-**D**) Densitometric data of phosphoproteins (normalized to pan proteins) were summarized from 3 mice per genotype in Fig. 4B, 4C, and 4D. Analyses were performed in 3 independent experiments. Data are presented as mean±S.D. of biological replicates.

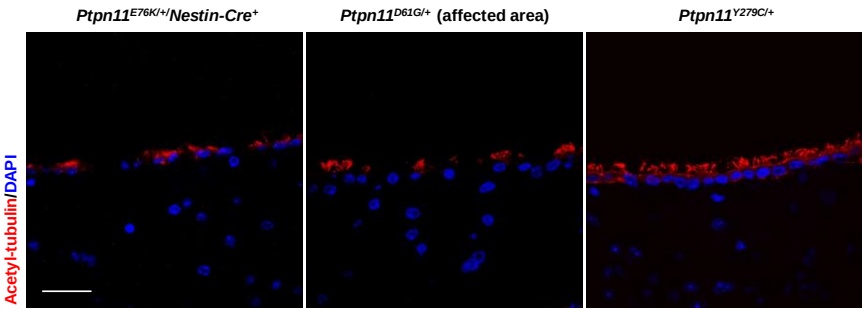

Fig. S7. Defects of ependymal cilia are proportionate to the catalytic activity of various mutant forms of SHP2. Brain sections prepared from *Ptpn11*$^{E76K/+}$*/Nestin-Cre*$^{+}$, *Ptpn11*$^{D61G/+}$, and *Ptpn11*$^{Y279C/+}$ mice (*n*=3 mice per genotype) at 12 months of age were processed for immunofluorescence staining of acetyl α-tubulin. Ependymal cilia on the walls of ventricles were examined (*Ptpn11*$^{D61G/+}$ mice showed ependymal cilia defects only on the third ventricular walls). Analyses were performed in 3 independent experiments. Representative images are shown. Scale bar, 50 μm.

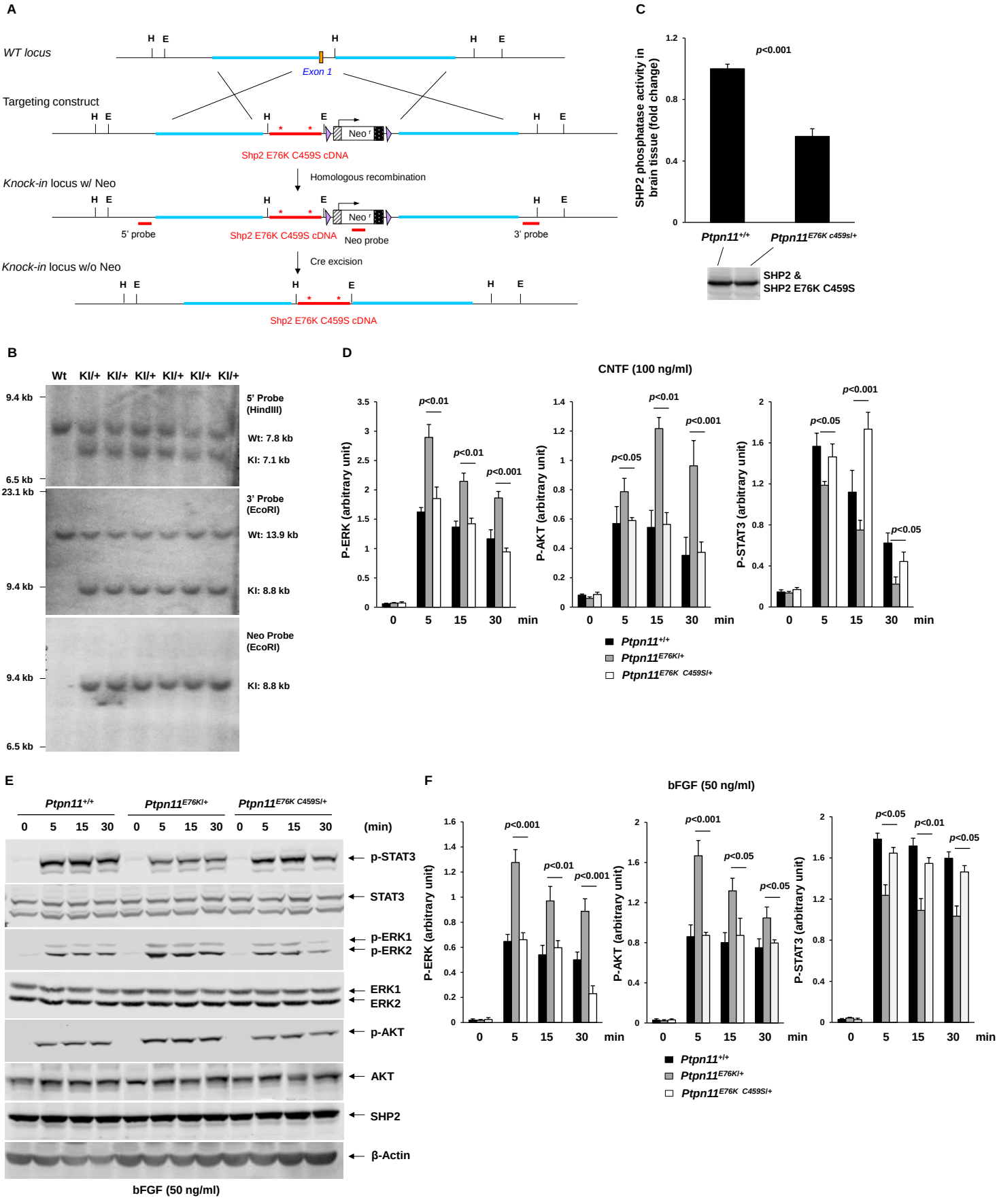
A
WT locus
Exon 1
Targeting construct
Neo r
Shp2 E76K C459S cDNA
Homologous recombination
Knock-in locus w/ Neo
5' probe
Neo probe
3' probe
Cre excision
Knock-in locus w/o Neo
B
Wt KI/+ KI/+ KI/+ KI/+ KI/+ KI/+
9.4 kb
6.5 kb
23.1 kb
5' Probe (HindIII)
Wt: 7.8 kb
KI: 7.1 kb
3' Probe (EcoRI)
Wt: 13.9 kb
KI: 8.8 kb
Neo Probe (EcoRI)
C
SHP2 phosphatase activity in brain tissue (fold change)
p<0.001
Ptpn11+/+
Ptpn11E76K c459s/+
SHP2 &
SHP2 E76K C459S
D
CNTF (100 ng/ml)
P-ERK (arbitrary unit)
P-AKT (arbitrary unit)
P-STAT3 (arbitrary unit)
min
Ptpn11+/+
Ptpn11E76KI/+
Ptpn11E76K C459S/+
E
Ptpn11+/+
Ptpn11E76KI/+
Ptpn11E76K C459S/+
(min)
p-STAT3
STAT3
p-ERK1
p-ERK2
ERK1
ERK2
p-AKT
AKT
SHP2
β-Actin
bFGF (50 ng/ml)
F
bFGF (50 ng/ml)

Fig. S8. Generation and characterization of *Ptpn11*$^{E76K,C459S/+}$ mice. (**A**) Gene-targeting strategy for generation of *Ptpn11*^{E76K,C459S} double mutation knock-in mice. (**B**) Genomic DNA extracted from targeting vector-transfected embryonic stem cell clones was digested with the indicated DNA restrictive enzymes followed by Southern blotting using the probe labeled with digoxigenin-11-dUTP following standard procedures. Wildtype (Wt) and *Ptpn11*$^{E76K\ \ C459S/+}$ (KI/+) clones were identified. (**C**) Brain tissues isolated from *Ptpn11*$^{E76K,C459S/+}$ and *Ptpn11*$^{+/+}$ littermates (*n*=3 mice per genotype) were lysed. SHP2 enzymatic activities in the lysates were assessed by the immunocomplex phosphatase assay. (**D**) Densitometric data of phosphoproteins (normalized to pan proteins) were summarized from 3 mice per genotype in Fig. 7E. (**E**) Neurospheres derived from *Ptpn11*$^{+/+}$*/Nestin-Cre*$^{+}$, *Ptpn11*$^{E76K/+}$*/Nestin-Cre*$^{+}$, and *Ptpn11*$^{E76K,C459S/+}$ mice (*n*=3 mice per genotype) were processed for analyses of bFGF-induced cell signaling, as described in Fig. 4B and 4D. (**F**) Densitometric data of phosphoproteins (normalized to pan proteins) were summarized from (**E**). Analyses in (**C**), (**D**), and (**E**) were performed in 3 independent experiments. Data are presented as mean±S.D. of biological replicates. Representative images are shown.